Stem Cell Research & Therapy

RESEARCH

Open Access

Melatonin-pretreated mesenchymal stem cell-derived exosomes alleviate cavernous fibrosis in a rat model of nerve injury-induced erectile dysfunction via miR-145-5p/TGF-β/Smad axis

Xiaolin Zhang[1†], Mengbo Yang[1†], Xinda Chen[1], Ming Zhang[1], Yiliang Peng[1] and Mujun Lu[1*]

Abstract

Background Cavernous nerve injury-induced erectile dysfunction (CNI-ED) is a common complication after radical prostatectomy. Conventional treatment approaches have had little success in treating the severe cavernous fibrosis which is a consequence of CNI-ED.

Methods Pre-treatment of adipose-derived stem cells with melatonin allows for the extraction of active exosomes (MT-hASC-EVs) from the conditioned medium. The therapeutic effects of MT-hASC-EVs were assessed in a rat model of CNI-ED, and the anti-fibrotic properties were evaluated. MicroRNA sequencing was used to identify specific microRNAs highly expressed in MT-hASC-EVs, and differential microRNAs were screened for regulatory pathways through target gene enrichment analysis. Finally, the conclusions from bioinformatics analysis were validated through in vitro experiments.

Results Intracavernous injection of MT-hASC-EVs significantly restored erectile function and reduced the extent of corpus cavernosum fibrosis in the CNI-ED rat model. MT-hASC-EVs promoted the proliferation and anti-apoptotic effects of corpus cavernosum smooth muscle cells (CCSMCs) in vitro. Mechanistically, MT-hASC-EVs inhibit fibrosis by delivering miR-145-5p, which targets TGF-β2/Smad3 axis.

Conclusions MT-hASCs-EVs can inhibit cavernous fibrosis and improve erectile function in a rat model of CNI-ED by targeting the miR-145-5p/TGF-β/Smad axis.

Keywords Melatonin, Mesenchymal stem cell, Exosome, CNI-ED, Cavernous fibrosis

[†]Xiaolin Zhang and Mengbo Yang these authors contributed equally to the work.

*Correspondence:
Mujun Lu
lumujun@sjtu.edu.cn
[1]Department of Urology and Andrology, Ren Ji Hospital, School of Medicine, Shanghai Jiao Tong University, NO. 145 Middle Shandong Road, Shanghai 200001, China

Introduction

Erectile dysfunction (ED) refers to the persistent or recurrent inability to achieve and maintain sufficient penile erection for satisfactory sexual intercourse [1]. The etiology of ED is complex, and cavernous nerve injury (CNI) is a significant contributing factor, commonly associated with pelvic surgery, pelvic fractures, and post-urethral injury surgeries [2]. CNI-induced ED following radical prostatectomy has an incidence rate as high as 63-94%, despite the use of nerve-sparing techniques [3]. During radical prostatectomy, unavoidable traction, compression, and vascular damage to the cavernous nerves lead to impairment and neurotrophic loss which results in reduced penile blood flow perfusion, leading to sustained hypoxia in the corpus cavernosum [3]. Subsequent smooth muscle atrophy occurs along with activation of TGF-β/Smad and RhoA/Rock pathways which lead to cavernous fibrosis [2, 4]. Traditional phosphodiesterase 5 inhibitors (PDE5i, e.g., tadalafil and sildenafil) have limited efficacy in treating CNI- ED due to insensitivity of corpora cavernosa tissue to nitric oxide (NO) resulting from smooth muscle cell loss and cavernous fibrosis [5, 6]. It is worth noting that while regeneration of cavernous nerves could be observed 28 days after CNI in a rat model, subsequent loss of smooth muscle cells and cavernous fibrosis were irreversible [7]. Therefore, prevention, alleviation, or even reversal of cavernous fibrosis represents an important therapeutic direction for managing CNI-ED.

In recent years, stem cells and their derivatives have become new treatment options for ED [8–10], among which extracellular vesicles (EVs) have gained favor among researchers due to their simplicity, convenience, and suitability for industrial production [11]. EVs are sac-like structures that cells release into the extracellular space [12–14]. Based on diameter and source, they can be divided into exosomes (50–100 nm) and microvesicles (100–1000 nm). As a carrier, EVs transport signal proteins, lipids, and nucleic acids, which can be endocytosed by distant target cells, thereby changing the biological behavior of the target cells and serving as a key factor in cell-to-cell signal communication [15]. Many reports have suggested that mesenchymal stem cell-derived EVs have a certain therapeutic effect on CNI-ED [16–19].

Melatonin is a hormone secreted by the pineal gland, primarily responsible for regulating biological rhythms and sleep-wake cycles [20]. In addition, melatonin has been found to have therapeutic effects on several fibrotic diseases including liver fibrosis [21], pulmonary fibrosis [22], and renal fibrosis [23], indicating its potential in counteracting cavernous fibrosis caused by CNI-ED. Furthermore, melatonin exhibits the ability to promote nerve regeneration [24], thereby improving erectile function through the protection and promotion of repair of cavernous nerves [25, 26]. Melatonin can regulate the behavior of MSCs and significantly enhance the therapeutic effects of MSCs-derived EVs in certain diseases. For example, melatonin-pretreated MSCs-derived EVs shows better protective effects against rat renal ischemia-reperfusion injury [27]; they also show stronger therapeutic effects in diabetic wound healing [28]. However, it is still unclear whether melatonin-pretreated MSCs-derived EVs can play a therapeutic role in fibrotic diseases.

In this study, we found that exosomes derived from melatonin-pretreated adipose mesenchymal stem cells (MT-hASC-EVs) exhibit high expression of miR-145-5p through which they can target the TGF-β2/Smad3 axis, inhibit corpus cavernosum fibrosis in the CNI-ED rat model, and subsequently promote the recovery of erectile function. This may represent a potential therapeutic approach for CNI-ED.

Materials and methods

Cell isolation, culture and identification

Human adipose stem cells (hASCs) were isolated from abdominal adipose tissues from healthy female liposuction as previously reported [29]. hASCs were resuspended in Minimum Essential Medium Alpha (α-MEM, Gibco, USA) supplemented with 10% fetal bovine serum (New Zealand Characterized Fetal Bovine Serum, Hyclone, SH30406.05) and 1% penicillin-streptomycin (Beyotime, CNH) and cultured at 37 ° C in a 5% CO_2 incubator. The medium was changed every 3 days. Cells were passaged when they reached 80% confluence. All cells used in the experiments were at passages 3 to 5. The differentiation properties and stem cell markers of hASCs have been identified in our previous reports [29].

The isolation of corpus cavernous smooth muscle cells (CCSMCs) was conducted as described previously [29]. In brief, after anesthesia by intraperitoneal injection of pentobarbital sodium (35 mg/kg), Sprague Dawley (SD) rats were euthanized by excess carbon dioxide. The hair from the lower abdomen to the perineal area was shaved. The surgical area was then adequately disinfected with iodophor. The foreskin and dorsal penile vessels were removed to obtain penile corpus cavernosum tissue. The corpus cavernosum tissue was washed in PBS and cut into small pieces of 1 to 2 mm. Segments were placed on 10-cm cell culture dishes (Corning, USA) containing a minimal volume of Dulbecco's minimum essential medium (DMEM, Gibco, USA) supplemented with 20% FBS and cultured at 37 ° C in a humidified atmosphere of 95% air and 5% CO2. After the explants were attached, more DMEM containing 10% FBS was added and tissue segments that had fallen off from the culture dish were removed. The cells were cultured in high-glucose DMEM (Gibco, USA), supplemented with 10% FBS (Hyclone,

SH30406.05, USA), 1% penicillin-streptomycin (Beyotime Biotechnology, China) at 37 °C and 5% CO2. The cells were frozen or passaged once 80–90% confluence was achieved. All cells used in the experiments were at passages 3 to 8.

Isolation and characterization of extracellular vesicles

An EV-free FBS was prepared by ultracentrifugation at 100 000 × g for 2 h at 4 °C and filtered with a 0.22 μm filter. When the ADSC at passage 3 to 5 reached an 80% density, cells were washed with PBS and cultured in culture medium supplemented with EV-free FBS for 48 h, while MT-hASCs were incubated with 10μM melatonin. The media were then collected, and exosomes were isolated through a multistep centrifugation. Dead cells, cell debris and microvesicles were removed at 300 g for 5 min, 3000 g for 10 min and 10,000 g for 30 min, respectively. The supernatant was then ultracentrifuged at 100 000 × g for 2 h (XP-90, Beckman Coulter, USA). The pellets were washed for three times and resuspended with PBS to obtain a suspension of hASC-EVs or MT-hASC-EVs. The total protein concentration of the MT-hASC-EVs and hASC-EVs was quantified using a micro bicinchoninic acid protein assay kit (Beyotime, CHN). In the in vitro cell experiments, both MT-hASC-EVs and hASC-EVs were treated at a concentration of 25 μg/mL. In the in vivo experiments, each rat in the treatment group (weighing ~ 250 g) were injected with 100ug of MT-hASC-EVs or hASC-EVs in 0.1mL PBS.

For EV characterization, the EV-positive markers CD81 (Abclonal, A5270, 1:1000), CD9 (Abclonal, A1703, 1:1000), and TSG101 (Abclonal, A2216, 1:1000), and the EV-negative marker, Calnexin (Abclonal, A15631, 1:1000), were identified by western blotting analysis. The size distribution of the EVs was determined using the NanoSight NS300 (Malvern, UK), according to the manufacturer's instructions. The ultrastructure and morphology of the EVs prepared by the Exosome-TEM-easy kit (101Bio, USA) were observed using transmission electron microscopy (TEM; Hitachi, JP).

In vivo experimental design

The work has been reported in line with the ARRIVE guidelines 2.0.

Generally, forty 8-week-old Sprague Dawley (SD) rats (males, weighing 250 g each) were used in this study. All rats were maintained on a 12 h light/12 h dark cycle and were acclimatized for at least 1 week before surgery and allowed free access to standard food and water. Operations and welfare in this study complied with international and Chinese local legislations and National Institutes of Health guide for the care and were guaranteed under the supervision of the Experimental Animal Ethical Committee of Ren Ji Hospital (KY2022-180-B).

Bilateral CNI was performed in 30 rats (CNI group), and the other 10 rats were subjected to only laparotomy (Sham group). The construction of the CNI-ED animal model was conducted as previously described [30]. After anesthesia by intraperitoneal injection of pentobarbital sodium (35 mg/kg), the rats were placed on an isothermal thermal pad. Hair above the abdomen and perineum was shaved with a hair clipper for better visualization. After disinfection with iodophor, a 2.5-cm midline lower abdominal incision was made to expose the pelvic ganglions (MPG) and cavernous nerves (CNs) on the surface of both sides of prostate. The CNs were isolated bilaterally and crushed 5 mm distal to the MPG of 90s using microforceps (Storz, Germany). Then, the CNI group was randomly divided into three groups of 10 rats each, which respectively received intracavernous injection of (1) PBS (0.1mL); (2) hASCs-EVs (100 μg in PBS 0.1 ml); (3) MT-hASC-EVs (100 μg in PBS 0.1 ml). The intracavernous injection method was performed as previously described [9]. In brief, the penis was exposed locally and a rubber tourniquet was applied at the base. After injection of 0.1 ml solution into the corpus cavernosum, the tourniquet was removed after 1 min and the penis was restored. Four weeks after the injection, the erectile function of the rats in each group was evaluated.

Erectile function evaluation

Penile erection is achieved by congestion of the corpus cavernosum, during which the intracavernous pressure (ICP) increases significantly. So the erectile function of rats can be objectively evaluated by detecting changes of ICP. However, ICP levels can be influenced by arterial pressure, hence it is necessary to simultaneously measure mean arterial pressure (MAP) and calculate the ratio between the two for standardization. The maximal ICP and real-time arterial pressure were recorded as previously described [29, 30]. 4 weeks after intracavernous injection, SD rats were anesthetized by intraperitoneal injection of pentobarbital sodium (35 mg/kg). A 26-gauge needle connected to a catheter inserted into one side of corpus cavernosum to measure the ICP while the other end of the catheter was connected to a data collection device (BL-420s, Chengdu Taimeng Software Co.Ltd., China) using a pressure transducer. After exposing the carotid artery of the other side, a 20-gauge cannula filled with heparin saline was punctured in the artery to measure the MAP, with the other end of the cannula connected to the BL-420s using a pressure transducer. The cavernous nerve of the other side was dissected and separated in the same way described above, and the CN was stimulated with electrodes with stimulus parameters set at 5 V, 25 Hz and 60 s duration. The ratio of maximal ICP to MAP during the process was considered as the objective measure of erectile function. At the end, the penis

was excised for further testing, and then the rats were euthanized with carbon dioxide.

Fluorescent labeling and in vitro tracing of EVs

hASC-EVs and MT-hASC-EVs were labeled with PKH67 dye (Maokang Biotechnology, China) according to the manufacturer's instructions. CCSMCs were incubated with PKH67-labeled EVs for 12 h at 37℃. Following fixation with 4% paraformaldehyde and stained with 40, 6-diamidino-2-phenylindole (DAPI, Invitrogen, USA), the cells were observed under the confocal laser scanning microscope (FV3000, Olympus, Japan).

CCSMC viability and proliferation

For cell viability evaluation, CCSMCs were seeded in a 96-well plate with a density of 2000 cells per well and incubated with hASC-EVs or MT-hASC-EVs. 24–48 h later, Cell Counting Kit-8 (Beyotime, China) was added to the medium and incubated at 37℃ for 2 h. Cell viability was assessed by OD value of each well using a microplate reader (Biotek, USA).

For EdU cell proliferation staining, CCSMCs were seeded in a six-well plate and pre-treated with hASC-EVs or MT-hASC-EVs for 24 h. Then, EdU cell proliferation staining was performed using an EdU kit (BeyoClick™ EdU Cell Proliferation Kit with Alexa Fluor 488, Beyotime, China) according to the manufacturer's instructions and nuclei were stained using DAPI(Beyotime, China). The fluorescence was detected using the fluorescence microscope (Olympus, Japan) and the cells in the proliferative phase were counted using Image J software.

Cell apoptosis assay

Annexin V-FITC/PI cell apoptosis detection kit (Yeasen Biology, China) was used to detect the level of apoptosis under different conditions. CCSMCs seeded in a six-well plate (Costar, United States) were pre-treated with hASC-EVs or MT-hASC-EVs for 24 h and then stimulated under hypoxia for 24 h in anaerobic jars with Anaerobic cultivation sets (AnaeroPack™, MGC, Japan). Subsequently, the cells were collected and stained with Annexin V-FITC and PI probe solution at room temperature for 15 min. The apoptosis rate was detected by Cytoflex (Beckman Coulter, United States).

The miRNA library construction and sequencing

Total RNA of hASC-EVs and MT-hASC-EVs was extracted by the MagZol (Magen, China) according to the manufacturer's protocol. The quantity and integrity of RNA yield was assessed by using the Qubit®2.0 (Invitvogen, USA) and Agilent 2200 TapeStation (Agilent Technologies, USA) separately. Briefly, RNAs were ligated with 3' RNA adapter, and followed by 5' adapter ligation. Subsequently, the adapter-ligated RNAs were subjected to RT-PCR and amplified with a low-cycle. Then the PCR products were size selected by PAGE gel according to instructions of NEBNext® Multiplex Small RNA Library Prep Set for Illumina® (Illumina, USA). The purified library products were evaluated using the Agilent 2200 TapeStation, The libraries were sequenced by HiSeq 2500(Illumina, USA) with single-end 50 bp at Ribobio Co. Ltd (Ribobio, China).

The raw reads were processed by filtering out containing adapter, poly ' N', low quality, smaller than 17nt reads by FASTQC to get clean reads. Mapping reads were obtained by mapping clean reads to reference genome of by BWA. miRDeep2 was used to identify known mature miRNA based on miRBase21 (www.miRBase.org) and predict novel miRNA. The expression levels were normalized by RPM, RPM is equal to (number of reads mapping to miRNA/number of reads in Clean data)×10^6. Differential expression between two sets of samples was calculated by edgeR algorithm according to the criteria of|log2(Fold Change)|≥1 and p-value < 0.05. TargetScan, miRDB, miRTarBase and miRWalk were used to predict targets gene of selected miRNA. R 4.3.1 and miRPath v.3 (https://dianalab.e-ce.uth.gr/html/mirpathv3/index.php?r=mirpath) [31] were used for further Gene Ontology (GO) and KEGG (Kyoto Encyclopedia of Genes and Genomes) pathway analysis.

Immunocytochemistry (ICC)

CCSMCs were seeded in 35 mm confocal dishes (Bioshark, China) and induced using 10ng/mL recombinant human TGF-β2 (Proeintech, HZ-1092, USA), while hASC-EVs or MT-hASC-EVs were co-incubated. After 48 h, CCSMCs were fixed with 4% paraformaldehyde (PFA) and permeabilized with 0.1% Triton X-100 (Sigma, USA). Blocking was performed with goat serum for 1 h, followed by incubation with TGF-β2 specific antibody (Ptoteintech, 19999-1-AP, 1:100) overnight. Then, the cells were incubated with green fluorescent secondary antibody (Proteintech, RGAR002, 1:200) for 1 h at room temperature. Nuclei were stained using DAPI (Invitrogen, USA). CCSMCs were observed under the confocal laser scanning microscope (Olympus, Japan) and the fluorescent intensity was valued by Image J software.

Transfection

Cell transfection was performed using Lipofectamine 3000 (Invitrogen, USA), according to the manufacturer's protocol. The miR-145-5p inhibitor and NC inhibitor, miR-145-5p mimics and NC mimics were obtained from Genomeditech (Shanghai, China), and their sequences were shown in Supplementary Table 2.

Extracellular vesicle transfection of miR-145-5p mimics or miR-145-5p inhibitor was performed using

Extracellular Vesicle RNA Loading Kit (Echo Biotech, China), according to the manufacturer's instructions.

Dual-luciferase reporter assay

The entire 3′-UTR fragments of *Tgfb2* and *Smad3* and the mutant form in which the potential miR-145-5p binding sites were mutated were inserted into PGL3-CMV-LUC vector, namely Rat_Tgfb2 WT, Rat_Tgfb2 mut, Rat_Smad3 WT and Rat_Smad3 mut, respectively. Plasmid profiles as well as sequences are shown in Supplementary Fig. 13 and Supplementary Table 5. These plasmids were respectively, co-transfected with miR-145-5p mimics or mimics NC into HEK293 cells. After 48 h, cells were collected and luciferase activity was measured using Dual-Luciferase Reporter Assay System (E1910, Promega, Madison, WI, USA).

Biological safety analysis

Biosafety analysis included both short-term (2 days) and long-term (3 weeks) assessments.

For the short-term assessment, 9 male SD rats weighing approximately 250 g were randomly divided into three groups ($n = 3$) and injected intracavernously with 0.1mL of PBS, hASC-EVs (100 μg in 0.1mL PBS) or MT-hASC-EVs (100 μg in 0.1mL PBS). Two days post-injection, blood was drawn from the rats' jugular veins to measure white blood cell (WBC) using a Blood Cell analyzer (TEK-VET3, TECOM, China). The rats were anesthetized with pentobarbital sodium (35 mg/kg) and euthanized with excess carbon dioxide, after which the corpus cavernosum tissue was isolated and assessed for Hematoxylin-Eosin (HE) staining.

For the long-term assessment, 9 male SD rats weighing approximately 250 g were randomly divided into three groups ($n = 3$) and injected intracavernously with 0.1mL of PBS, hASC-EVs (100 μg in 0.1mL PBS) or MT-hASC-EVs (100 μg in 0.1mL PBS) on the first day of each week. Three weeks after the initial injection (a total of three injections were given), blood was drawn from the rats' jugular veins to test for Aspartate aminotransferase (AST), Alanine aminotransferase (ALT), Creatinine (CR) and Blood urea nitrogen (BUN) using a Blood biochemistry analyzer (BK-280, BIOBASE, China). The rats were anesthetized with pentobarbital sodium (35 mg/kg) and euthanized with excess carbon dioxide, after which the corpus cavernosum and major organs (heart, liver, kidneys, lungs, and spleen) were isolated and assessed for pathological changes using HE staining.

Histological and immunohistochemical analysis

For Hematoxylin-Eosin (HE) staining and Masson's trichrome staining, the tissues were fixed in 4% paraformaldehyde overnight, which were subsequently dehydrated and embedded in paraffin. Next, the paraffin-embedded tissue was cut into 4-micron sections for staining. After gradient dehydration with xylene, the sections were stained with an HE staining kit (Solarbio, China) or a Masson trichrome staining kit (Solarbio, China). Stained sections were observed under microscope. To assess the degree of cavernous fibrosis indicated by Masson trichrome staining, the red area representing smooth muscle fibers and the blue area representing collagen fibers were calculated separately by Image J software. The ratio of smooth muscle fiber area to collagen fiber area was considered as an index negatively correlated with the degree of cavernous fibrosis.

For immunohistochemical staining, penile tissue sections were rehydrated, and antigen retrieval was performed. The sections were blocked with goat serum for 60 min, then incubated with anti-Desmin antibodies (Proteintech, 16520-1-AP, 1:500) overnight. Then, Max-Vision HRP-Polymer immunohistochemistry kit (Maxim, China) was used and the sections were developed in color with diaminobenzidine (DAB). Sections were then counterstained with hematoxylin. Stained sections were observed under microscope and analyzed using Image J software.

Real-time PCR

The EZ-press RNA Purification Kit (EZB, USA) was used to extract mRNA from the ASCs and CCSMCs. Exosome RNA Purification Kit (EZB, USA) was used to extract total RNA from EVs. TRIzol Reagent (Invetrogen, USA) was used to extract mRNA from tissue. A reverse transcription kit (TaKaRa, Japan) was used to synthesize complementary DNA from mRNA. An miRNA 1st Strand cDNA Synthesis Kit (by stem-loop) (Vazyme, China) was used to synthesize complementary DNA from microRNA. The ChamQ Universal SYBR qPCR Master Mix (Vazyme, China) was used to and perform quantitative real-time PCR, according to the manufacturer's instructions. ACTB and U6 were used as internal controls. The LightCycler 480 real-time PCR system (Roche Diagnostics, Indianapolis, IN, USA) was used for detection. The primers used are listed in Supplementary Table 1.

The Ct values of each gene in the samples were converted to relative expression levels (with the control group in each experiment set as 1) for statistical analysis. The formula is as follows:

(1) ΔCt = Ct (gene of interest) − Ct (housekeeping gene);
(2) ΔΔCt = ΔCt (treated sample) − ΔCt (control sample);
(3) Relative expression level = 2^(-ΔΔCt).

Western blots

Proteins were extracted using RIPA Lysis Buffer (Beyotime, China) according to the manufacturer's

instructions. Assays for RhoA activation were performed by using Active GTPase Pull-Down and Detection Kits (ThermoFisher, USA).The protein concentration was detected using a Bicinchoninic Acid Protein Assay Kit (Beyotime, China). The Protein solution and SDS-PAGE Protein Sample Loading Buffer (Beyotime, China) were mixed and denatured by heating at 95 ° C. 10 μg of proteins were used for electrophoresis per lane. After electrophoresis, the proteins were transferred onto polyvinylidene difluoride membranes. The membranes were blocked with Tris-buffered saline-Tween (with 5% skim milk) and incubated at 4 °C overnight with primary antibodies against β-actin (Proeintech, 66009-1-Ig, 1:20000), TGF-β2(Proteinteech, 19999-1-AP, 1:1000), Smad3 (Abclonal, A19115, 1:20000), p-Smad3 (Cell Signaling Technology, #9520, 1:1000), COL1A1 (Abclonal, A1352, 1:1000), COL3A1 (Abclonal, A3795, 1:2000), RhoA (Proteintech, 10749-1-AP, 1:1000), Rock1 (Proteintech, 21850-1-AP, 1:5000), p-Rock1 (ThermoFisher, PA5-114634, 1:1000), ERK1/2 (Proteintech, 11257-1-AP, 1:2000), p-ERK1/2 (Proteintech, 28733-1-AP, 1:1000), AKT (Proteintech, 10176-2-AP, 1:2000), p-AKT (Proteinteck, 66444-1-Ig, 1:2000). After hybridization with the secondary antibody (Proteinteh, 1:10000), bands were observed with enhanced chemiluminescence substrates (Millipore, MA) under a chemiluminescence imaging system (Bio-Rad, USA). The grayscale values of the bands were calculated using Image Lab software.

Statistical analysis

All quantitative data were expressed as the mean ± standard deviation. Statistical analyses were performed using GraphPad Prism v9.0 software. The normality of data distribution was assessed by the Shapiro-Wilk test. Homogeneity of variance was assessed by the F-test for two-group comparisons and by the Brown-Forsythe test for multiple group comparisons. Significant differences were determined using two-tailed unpaired Student's t-tests for two-group comparisons and one- or two-way analysis of variance (ANOVA) with the Sidak's test for multiple group comparisons. Details on the statistics used can be found in the figure legends. Differences were considered statistically significant at $p < 0.05$.

Results

Isolation and characterization of melatonin-pretreated adipose mesenchymal stem cell-derived EVs

Primary adipose mesenchymal stem cells were isolated from human adipose tissue. After 48 h of treatment with 10μM Melatonin, the conditioned medium was collected, from which MT-hASC-EVs were isolated (Fig. 1A). Both hASCs and melatonin-pretreated hASCs showed typical spindle and fibroblast-like morphologies (Fig. 1B). The levels of growth factors secreted by hASCs were detected by RT-PCR (Fig. 1C). After Melatonin treatment, the mRNA expression levels of various growth factors in hASCs increased, among which the expression level of SHH (Sonic Hedgehog) increased most significantly as early as 2–4 h of Melatonin treatment. In addition, the expression levels of PDGF, HGF and PGF were also significantly increased after melatonin pretreatment.

hASC-EVs and MT-hASC-EVs were isolated from the conditioned medium of hASCs and melatonin-treated hASCs respectively. Western Blot revealed that hASC-EVs and MT-hASC-EVs both highly expressed CD81, CD9, and the endosomal marker TSG101, but rarely expressed the endoplasmic reticulum marker Calnexin (Fig. 1D), which is in line with the typical marker expression of exosomes. Nanoparticle Trafficking Analysis (NTA) detection showed that the particle sizes of hASC-EVs and MT-hASC-EVs were mostly distributed in the range of 50–200 nm, with a main peak at about 110 nm (Fig. 1E). There was also no difference in mean particle size (Fig. 1F). Both hASC-EVs and MT-hASC-EVs had a typical cup-like shape under transmission electron microscope (TEM) (Fig. 1G). These results proved that EVs from hASCs and MT-hASCs were successfully isolated and characterized, while the pretreatment of melatonin had no significant effect on the markers, morphology, and particle size distribution of hASC-EVs.

Intracavernous injection of MT-hASC-EVs could restore erectile function and reduce cavernous fibrosis in a rat model of CNI-ED

In order to evaluate the therapeutic effects of MT-hASC-EVs on CNI-ED, we utilized a rat model of CNI-ED established through bilateral cavernous nerve crush, following which both types of EVs were administered via intracavernous injection. At 4 weeks post-treatment, the erectile function was assessed by measuring intracavernous pressure (ICP) and mean arterial pressure (MAP) (Fig. 2A and B). There were no significant differences in MAP among all groups. The successful establishment of CNI-ED model was confirmed by a significant decrease of ICP/MAP ratio in the PBS group compared with the sham group. Intracavernous injection of hASC-EVs or MT-hASC-EVs could restore the ICP/MAP ratio to a certain extent. Notably, the therapeutic effects of MT-hASC-EVs were more pronounced compared to that of hASC-EVs. As a complement, we compared the effects of MT-hASC-EVs with the classic therapeutic drug sildenafil (Supplementary Fig. 1). In CNI-ED rats, the elevation of ICP/MAP was not significant after oral administration of sildenafil citrate 2 h before testing, which may be attributed to the decreased sensitivity to nitric oxide (NO) due to cavernous fibrosis and reduced smooth muscle content. However, rats that received intracavernous injection of MT-hASC-EVs showed a more pronounced recovery

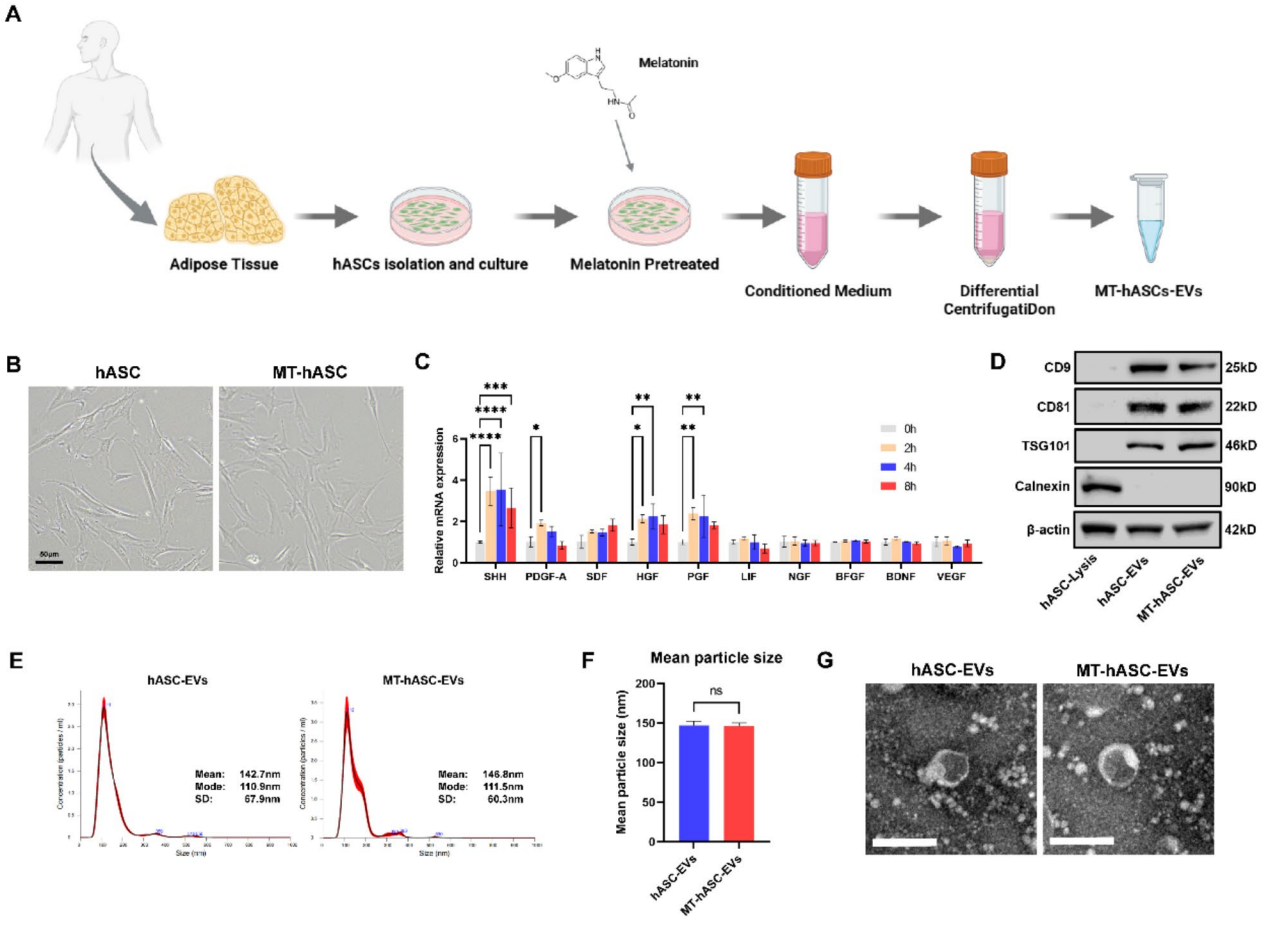

Fig. 1 Isolation and characterization of MT-hASC-EVs. **A**) Schematic diagram for the isolation of hASCs and purification of MT-hASC-EVs. **B**) Microscopic morphology of hASCs and MT-hASCs (Scale bar = 50 μm). **C**) RT-PCR analysis of the mRNA level of several growth factors of hASCs after melatonin treatment for 2 h, 4 h and 8 h ($n = 3$, biological replicates). **D**) Western Blot analysis of exosome-positive markers (CD9, CD81, and TSG101) and exosome-negative marker (Calnexin) of hASC-EVs and MT-hASCs-EVs compared with hASC lysis. Original Western Blot bands are presented in Supplementary Fig. 4. **E**) Particle size distribution of the hASC-EVs and MT-hASC-EVs measured by nanoparticle tracking analysis (NTA). **F**) The statistical analysis of the mean particle size of hASC-EVs and MT-hASC-EVs detected by NTA ($n = 5$, biological replicates). **G**) Transmission electron microscopy (TEM) analysis of hASC-EVs and MT-hASC-EVs showing the typical morphology (scale bar = 0.2 μm). Data are presented as the mean ± SD. Statistical analyses are performed by Student's t test (F) and Two-way ANOVA with the Sidak's test for multiple group comparisons (**C**). *, $p < 0.05$; **, $p < 0.01$; ***, $p < 0.001$; ****, $p < 0.0001$; ns, no significance

effect on ICP/MAP compared to sildenafil, suggesting the great potential of MT-hASC-EVs.

Cavernous fibrosis is one of the most severe pathological changes of CNI-ED, making it a major factor contributing to the refractory of the disease, so we focused on the degree of cavernous fibrosis among all groups. The Masson staining results showed. obvious collagen fiber accumulation and a significant decrease in the ratio of muscle fibers to collagen fibers in PBS group. hASC-EVs and MT-hASC-EVs could alleviate such phenomenon to some extent, with the therapeutic effect of MT-hASC-EVs being more obvious, suggesting the stronger anti-fibrotic effects of MT-hASC-EVs (Fig. 2C and D). Immunohistochemistry was used to evaluate the content of cavernous smooth muscle, and the results were consistent with the Masson staining results, with significant loss of Desmin + muscle fiber in PBS group and the highest smooth muscle level in MT-hASC-EV group (Fig. 2E and F). Chronic hypoxia caused by long-term low perfusion after CNI can activate the TGF-β/Smad pathway and induce cavernous nerve fibrosis. Therefore, Western Blot was used to reveal that MT-hASC-EVs could most significantly reduce the protein level of TGF-β2 and p-Smad3 in cavernous nerve tissue after CNI, thereby reducing the expression of Collagen I (Fig. 2G and H). Similarly, RT-PCR also revealed that MT-hASC-EVs had a significant down-regulation effect on the mRNA levels of *Tgfb2* and *Col1a1* (Fig. 2I). These results suggest that MT-hASC-EVs have good effects in relieving

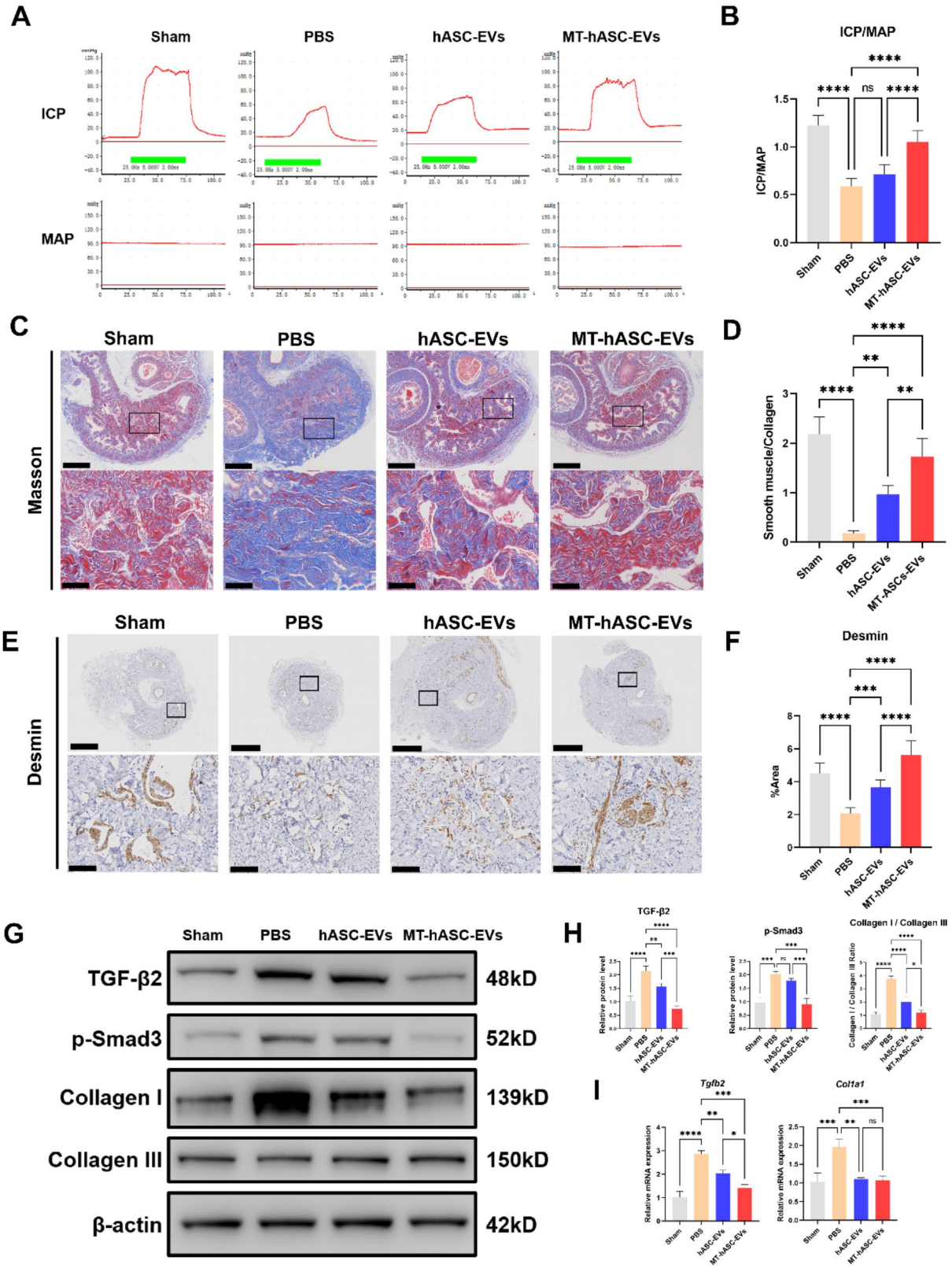

Fig. 2 (See legend on next page.)

(See figure on previous page.)

Fig. 2 MT-hASC-EVs improved erectile function and alleviated cavernous fibrosis in CNI-ED rats. **A**) Changes of ICP and MAP curves after electrical stimulation of the cavernous nerve in Sham group, PBS group, hASC-EVs group and MT-hASC-EVs group 28 days after CNI and administration. The green curves show the duration of the electrical stimulation. **B**) Statistical analysis of the relative ratio of ICPmax to MAP in four groups ($n=6$, biological replicates). **C**-**D**) Masson's trichrome staining of corpus cavernous tissue and the statistical analysis of the smooth muscle/collagen ratios of the four groups ($n=6$, biological replicates). Scale bar = 500 μm for the upper row of images. Scale bar = 100 μm for the lower row of images. The region corresponding to the images of the lower row is marked with a black box in the images of the upper row. **E**-**F**) Immunohistochemical (IHC) staining of Desmin in the corpus cavernosum tissue of the four groups and the statistical analysis of the density of Desmin ($n=6$, biological replicates). Scale bar = 1 mm for the upper row of images. Scale bar = 100 μm for the lower row of images. The region corresponding to the images of the lower row is marked with a black box in the images of the upper row. **G**-**H**) Western Blot analysis of the relative protein level of TGF-β2, p-Smad3, Collagen I and Collagen III in the corpus cavernosum of four groups ($n=3$, biological replicates). Original Western Blot bands are presented in Supplementary Fig. 5. **I**) RT-PCR analysis of the relative mRNA level of *Tgfb2* and *Col1a1* in the corpus cavernosum of four groups ($n=3$, biological replicates). Data are presented as the mean ± SD. Statistical analyses are performed by One-way ANOVA with the Sidak's test for multiple group comparisons (B, D, F, H and I). *, $p<0.05$; **, $p<0.01$; ***, $p<0.001$; ****, $p<0.0001$; ns, no significance

CNI-induced cavernous fibrosis by downregulating the TGF-β/Smad pathway.

MT-hASC-EVs could promote the proliferation of CCSMCs and reduce cell apoptosis in vitro

At the in vivo level, MT-hASC-EVs significantly increased the content of cavernous smooth muscle. To elucidate the mechanism, primary corpus cavernous smooth muscle cells (CCSMCs) were isolated from rat corpus cavernosum for the in vitro experiments. Both PKH67-labeled hASC-EVs and MT-hASC-EVs added to the culture supernatant were significantly up-taken by CCSMCs after 12 h (Fig. 3A). After incubation for 24 h, both MT-hASC-EVs and hASC-EVs significantly enhanced the cell viability of CCSMCs, with a stronger effect observed for MT-hASC-EVs. The effect became more pronounced after 48 h (Fig. 3B). When EdU was added to the culture medium, a higher number of EdU-positive cells was detected in CCSMCs after incubation with MT-hASC-EVs (Fig. 3C and D), indicating that MT-hASC-EV treatment promoted CCSMC proliferation. Furthermore, given that low oxygen-induced ROS damage is a key factor in CNI-ED progression, we stimulated CCSMCs with hypoixa and measured apoptosis rates under different treatment conditions. After hypoxia treatment, the apoptosis rate of CCSMCs significantly increased, while both MT-ASC-EVs and ASC-EVs had a certain inhibitory effect on CCSMC apoptosis, with the former being more significant (Fig. 3E and F). Taking all above account, CCSMCs can enhance cell proliferation after uptaking MT-ASC-EVs, while reducing cell apoptosis induced by hypoxia.

High-throughput sequencing revealed that the microRNAs in MT-hASC-EVs can target the TGF-β/Smad axis

EVs contain a large number of microRNAs, as one of the most important effectors in EVs. EVs can target specific mRNAs by delivering microRNAs to target cells and regulate protein expression specifically, thereby achieving the regulation of cell functions. Therefore, microRNAs specifically enriched in MT-hASC-EVs were screened by high-throughput sequencing. Among the co-expressed microRNAs, we selected those with a|Log2(FoldChange)|>1 and $p<0.05$ as the screening conditions to screen for differentially expressed microRNAs, ultimately obtaining 12 upregulated microRNAs and 8 downregulated microRNAs, which were displayed in the volcano plot (Fig. 4A) and heatmap (Fig. 4B).

microRNAs specifically target mRNAs to exert negative regulation, so we focused on the functional enrichment of target genes of 12 up-regulated microRNA. Using the prediction results from miRTarBase or the common prediction results from miRDB, miRWalk, and TargetScan as candidate target genes for the 12 upregulated microRNAs, a total of 4,928 target genes were identified(Supplementary Table 3). Gene Ontology (GO) enrichment analysis and Kyoto Encyclopedia of Genes and Genomes (KEGG) enrichment analysis were performed on these target genes. In the GO enrichment analysis, several enriched terms were related to "decreased oxygen levels", suggesting significant regulatory roles in cellular responses to hypoxia of these microRNAs, and it is worth noting the term "response to transforming growth factor beta" was also enriched, which is strongly related to hypoxia-induced cavernous fibrosis(Fig. 4C). Consistent with that, these target genes were enriched in the "TGF-beta signaling pathway" in KEGG enrichment analysis (Fig. 4D). In summary, the microRNA sequencing and target gene enrichment analysis suggest that the microRNAs enriched in MT-ASC-EVs may have played a therapeutic role in CNI-ED by targeting the TGF-beta pathway, which is consistent with the observation of downregulation of TGF-beta pathway-related proteins in the in vivo experiments.

MT-hASC-EVs could reduce the fibrosis of CCSMCs in vitro by inhibiting the TGF-β pathway

Subsequently, the results of microRNA sequencing and bioinformatics analysis were validated through a series of in vitro experiments. CCSMCs were treated with TGF-β (10ng/mL) for 48 h to induce fibrosis, and hASC-EVs or MT-ASC-EVs were simultaneously co-incubated. RT-PCR detection indicated that the mRNA level of *Tgfb2* was significantly decreased after MT-ASC-EVs

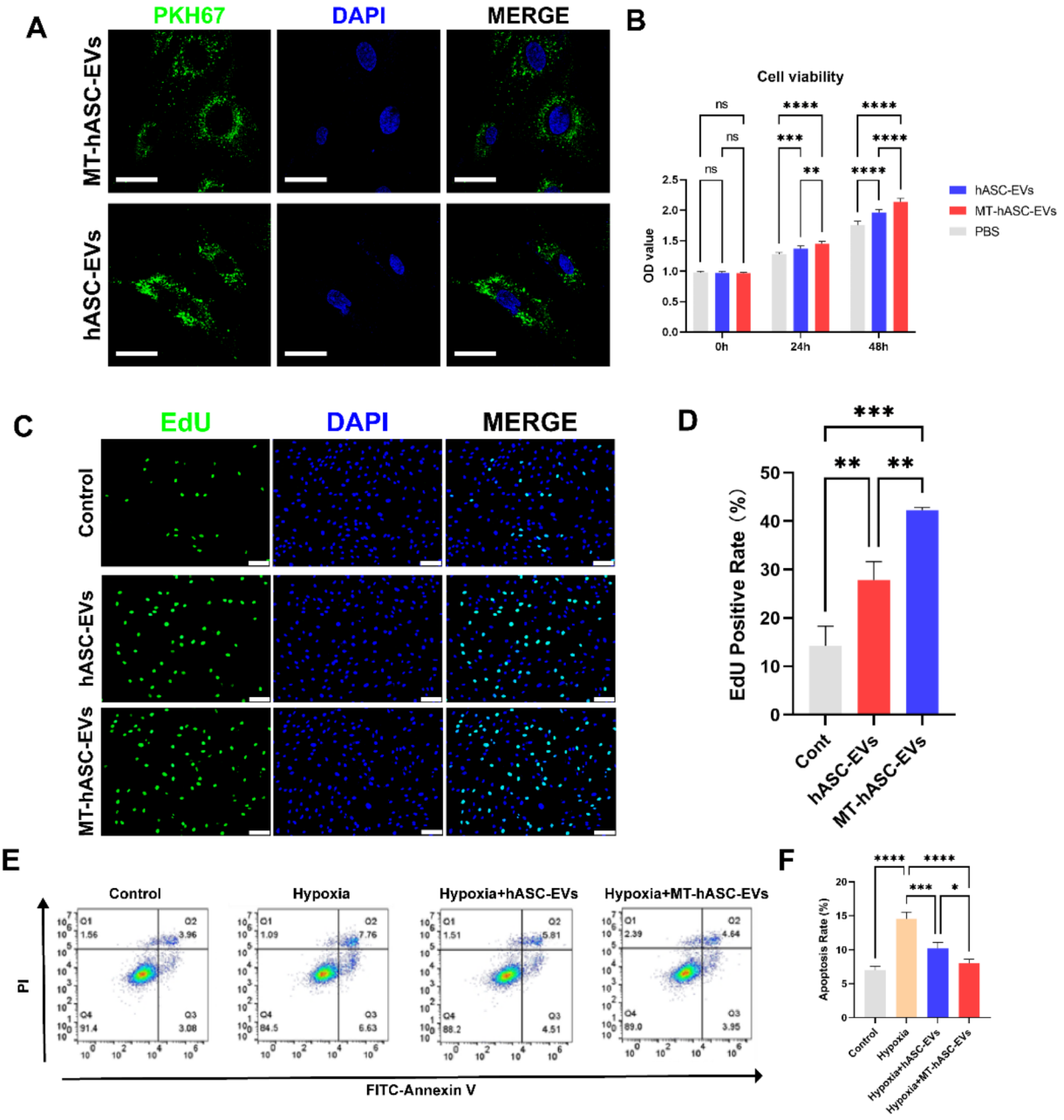

Fig. 3 MT-hASC-EVs could promote the proliferation and reduce the hypoxia-induced apoptosis of CCSMCs. **A**) Laser scanning confocal microscopy images of PKH67-labeled hASC-EVs and MT-hASC-EVs taken up by CCSMCs (scale bar = 20 μm). **B**) Effects of hASC-EVs and MT-hASC-EVs on cell viability of CCSMCs at 0 h, 24 h and 48 h indicated by CCK8 assay ($n = 6$, biological replicates). **C**-**D**) EdU staining of CCSMCs treated with hASC-EVs and MT-hASC-EVs for 24 h (scale bar = 100 μm) as well as the statistical analysis of the EdU-positive rate.($n = 3$, biological replicates) **E**-**F**) Flow cytometry analysis of hypoxia-induced apoptosis of CCSMCs as indicated by AnnexinV-PI double staining after treatment with hASC-EVs or MT-hASC-EVs ($n = 3$, biological replicates). The apoptosis rate calculation included early apoptosis in the Q3 quadrant as well as late apoptosis in the Q2 quadrant. Data are presented as the mean ± SD. Statistical analyses are performed by One-way (**D** and **F**) or Two-way (**B**) ANOVA with the Sidak's test for multiple group comparisons. *, $p < 0.05$; **, $p < 0.01$; ***, $p < 0.001$; ****, $p < 0.0001$; ns, no significance

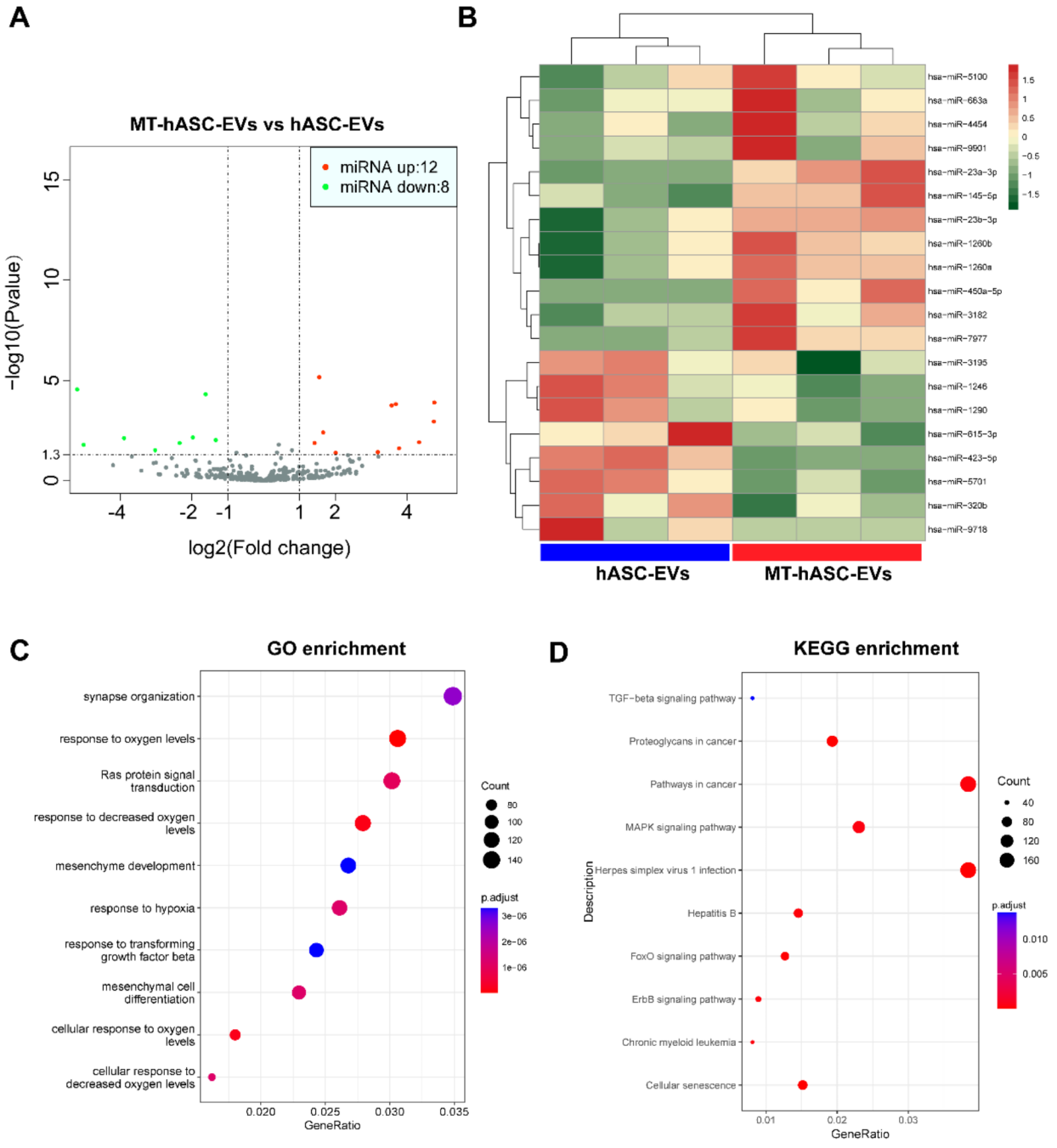

Fig. 4 Differences in microRNA expression between MT-hASC-EVs and hASC-EVs indicated by high THROUGHPUT Analysis. **A**) Volcano plots showing the differentially expressed microRNAs between MT-hASC-EVs and hASC-EVs. **B**) Heatmap showing the differential expression levels of miRNAs between MT-hASC-EVs and hASC-EVs. **C**-**D**) Significant enrichment of target genes of up-regulated miRNAs in GO analysis (**C**) and KEGG signaling pathways(**D**). Number of target genes in each pathway (indicated by circle diameters), and significance of enrichment (indicated by blue/red colors) are shown

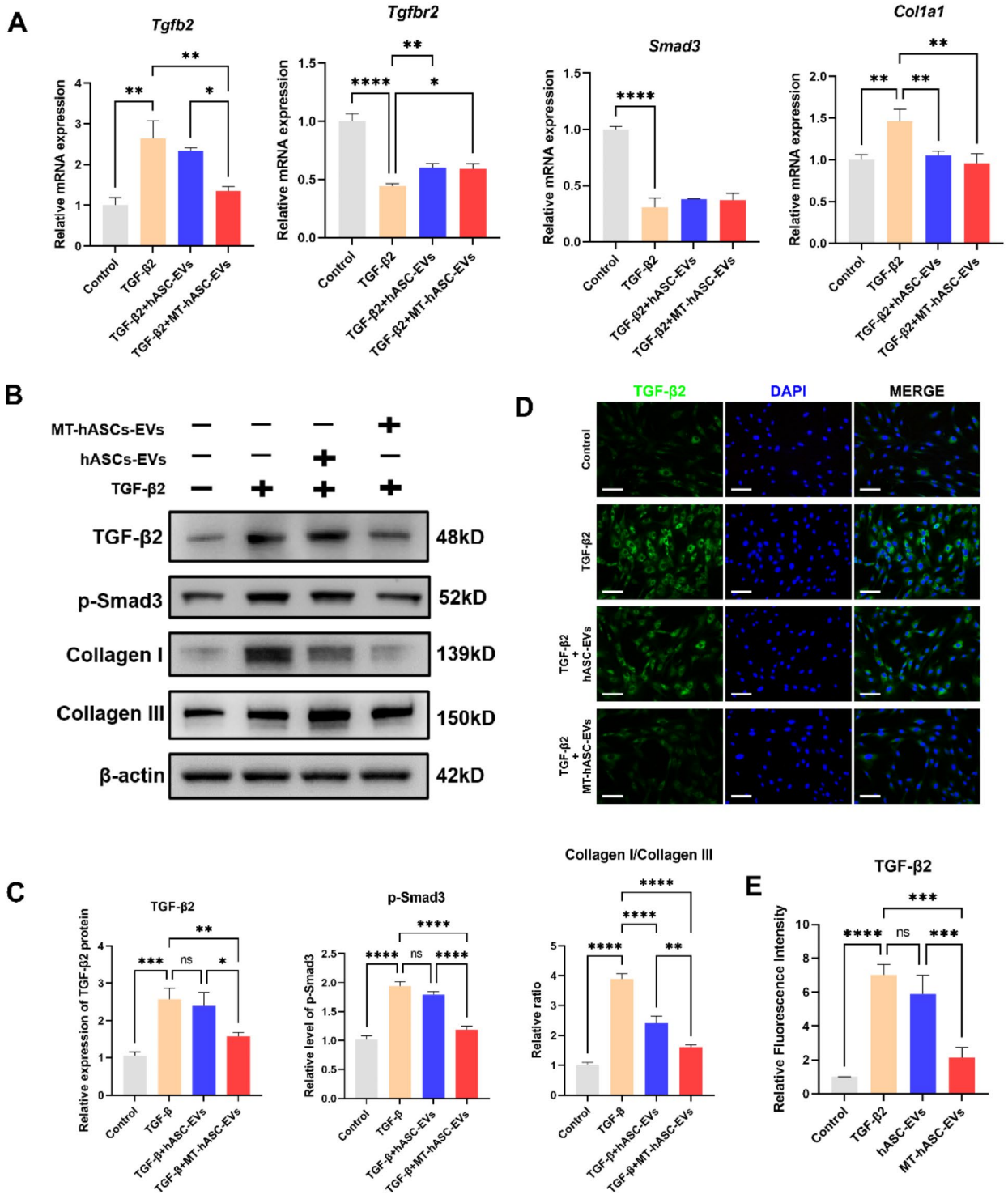

Fig. 5 MT-hASC-EVs could inhibit the activation of TGF-β pathway and fibrosis of CCSMCs in vitro. **A**) RT-PCR analysis showing relative mRNA levels of *Tgfb2*, *Tgfbr2*, *Smad3* and *Col1a1* of TGF-β-stimulated CCSMCs after incubation with hASC-EVs and MT-hASC-EVs.($n = 3$, biological replicates). **B**-**C**) Western Blot analysis of protein levels of TGF-β2, phosphorylated Smad3, Collagen I/Collagen III in CCSMCs ($n = 3$, biological replicates). Original Western Blot bands are presented in Supplementary Fig. 6. **D**-**E**) Immunofluorescence analysis of TGF-β2 in TGF-β-stimulated CCSMCs incubated with hASC-EVs or MT-hASC-EVs and statistical analysis of fluorescence intensity ($n = 3$, biological replicates, scale bar = 80 μm). Data are presented as the mean ± SD. Statistical analyses are performed by One-way ANOVA with the Sidak's test for multiple group comparisons (**A**, **C** and **E**). *, $p < 0.05$; **, $p < 0.01$; ***, $p < 0.001$; ****, $p < 0.0001$; ns, no significance

treatment, while the effect of ASC-EVs was not obvious (Fig. 5A). However, both of them could downregulate the mRNA level of Col1a1 and this may indicate both of the EVs contain microRNAs targeting the mRNA of Col1a1, rather than simply downregulating the expression of Col1a1 through the TGF-β pathway. Western Blot detection revealed that the levels of TGF-β2 and phosphorylated Smad3 in CCSMCs were significantly downregulated after MT-ASC-EVs treatment compared with the TGF-β2 group and hASC-EVs group. As for the evaluation index of fibrosis, CollagenI/CollagenIII, MT-hASC-EVs also showed more excellent anti-CCSMCs fibrosis effects (Fig. 5B and C). Consistent with that, in the ICC experiment, lower TGF-β2 fluorescence signals were detected in CCSMCs after MT-hASC-EVs treatment (Fig. 5D and E). It should also be noted that after the activation of the TGF-β pathway, in addition to stimulating canonical Smad-related pathways, it can also cross-talk with RhoA/Rock, PI3K/AKT, MAPK, and other pathways, collectively referred to as non-canonical pathways [4, 32]. As a supplement, Western Blot analysis revealed that MT-hASC-EVs significantly inhibit the activation of RhoA/Rock1, AKT, and ERK1/2 induced by TGF-β in CCSMCs (Supplementary Fig. 2). Combining the above results, after MT-hASC-EVs treatment, the activation level of the TGF-β pathway in CCSMCs was significantly downregulated, which may be an important mechanism for the anti-fibrosis effects of MT-hASC-EVs.

MT-hASC-EVs inhibit TGF-β2 and Smad3 expression through miR-145-5p

To further identify the core microRNAs that play a pivotal role among the differentially expressed miRNAs identified in the microRNA sequencing analysis, KEGG enrichment analysis was conducted on the upregulated miRNAs using the miRPath v3.0 software, a tool that can show the correspondence between enriched pathways and microRNAs (Fig. 6A). The results indicated that, among all upregulated miRNAs, miR-145-5p (targeting 12 genes), as well as miR-23b-3p and miR-23a-3p (both targeting 15 genes), were significantly enriched in the TGF-β signaling pathway (Supplementary Table 4). To validate these results, RT-PCR was first performed to assess the expression of miR-145-5p, miR-23a-3p, and miR-23b-3p in hASCs. Following a 48-hour treatment with 10 μM melatonin, a significant upregulation of these three miRNAs in hASCs was observed (Fig. 6B). Similarly, MT-hASC- EVs exhibited significantly higher expression levels of these three miRNAs compared to hASC-EVs (Fig. 6C). Given that the upregulation of miR-145-5p was particularly pronounced, we chose to focus our subsequent validation efforts on this specific microRNA. After treating CCSMCs with both types of EVs, RT-PCR analysis revealed that MT-hASC-EVs significantly increased the expression level of miR-145–5p (Fig. 6D).

TargetScan version 8.0 (https://www.targetscan.org/vert_80/) predicted binding sites for miR–145–5p within the 3' untranslated region (UTR) of rat *Tgfb2* at a 7mer-A1 site and within rat *Smad3* at an 8mer site which are illustrated in Fig. 6E. Dual luciferase reporter assays were performed to determine whether *Tgfb2* and *Smad3* serve as direct targets for regulation by miR–145–5p. The results demonstrated that co-transfection with a mimic for mir–145–5p led to a significant reduction in luciferase activity from both *Tgfb2* WT and *Smad3* WT constructs, while no significant changes were observed for *Tgfb2* mut or *Smad3* mut constructs (Fig. 6F), which confirmed the specific targeting. For further verification, transfection with miR – 145 – 5p mimics into TGF-β-stimulated CCSMCs resulted in marked down-regulation of the protein level of TGF – β2 and Smad3; conversely, transfection with miR – 145 – 5p inhibitor significantly up-regulated TGF-β2 and Smad3 (Fig. 6G and H).

While miR-145-5p alone can indeed inhibit the TGF-β2/Smad3 pathway, considering the complexity of the constituents within extracellular vesicles, it is crucial to further validate the specificity of miR-145-5p in the anti-fibrotic effects of MT-hASC-EVs. Transfection of miR-145-5p inhibitor into MT-hASC-EVs can significantly reduce their inhibitory effects on the TGF-β2/Smad3 pathway and fibrosis in CCSMCs (Fig. 6I and J). Similarly, transfection of miR-145-5p mimics into hASC-EVs can significantly enhance their inhibitory effects on the TGF-β2/Smad3 pathway and fibrosis (Supplementary Fig. 3). In summary, miR-145-5p is indeed the specific core factor in MT-hASC-EVs that plays a critical role in inhibiting the TGF-β2/Smad3 pathway and exerting anti-fibrotic effects.

MT-hASC-EVs showed good biological safety in both short-term and long-term assessment

CNI-ED and cavernous fibrosis are a chronic process and require long-term therapeutic follow-up, which means the in vivo safety of MT-hASC-EVs is critical. In the short-term safety evaluation, there was no significant change in the WBC levels of rats two days after intracavernous injection of hASC-EVs and MT-hASC-EVs (Fig. 7A), and HE staining also indicated no significant infiltration of immune cells in the corpus cavernosum tissue (Fig. 7F). After weekly injections for three consecutive weeks, there was no obvious change in liver function (AST, ALT) and kidney function (CR, BUN) indicators among all treatment groups (Fig. 7B-E). HE staining

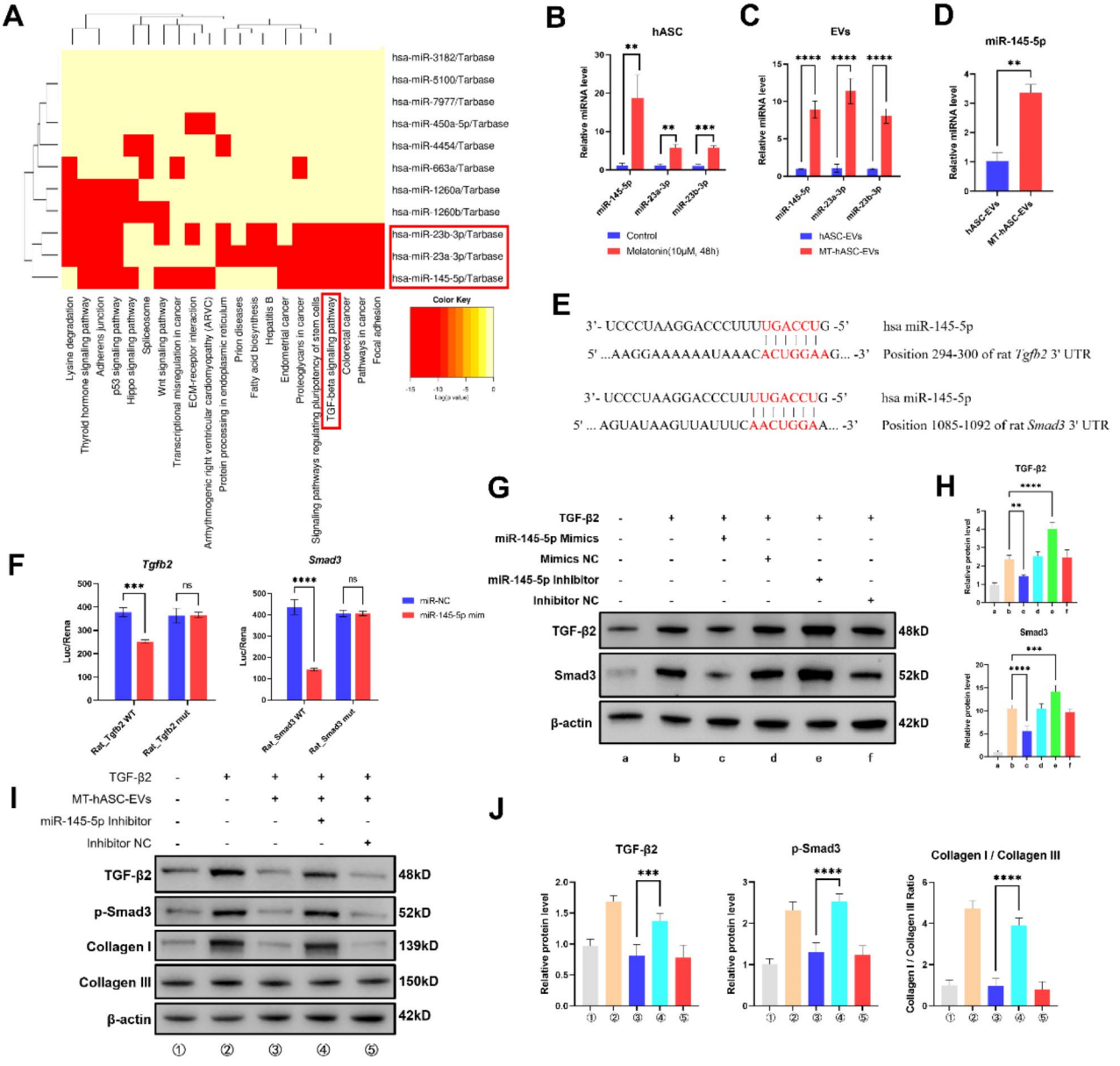

Fig. 6 MT-hASC-EVs could down-regulate TGF-β2/Smad3 pathway through miR-145-5p. **A**) KEGG enrichment analysis of up-regulated miRNAs of MT-hASC-EVs by miRPath v3.0. **B**) RT-PCR analysis showing the relative expression levels of miR-145-5p, miR-23a-3p and miR-23b-3p in hASCs after treatment of melatonin (n = 3, biological replicates). **C**) RT-PCR analysis showing the relative expression levels of miR-145-5p, miR-23a-3p and miR-23b-3p in hASC-EVs and MT-hASC-EVs (n = 3, biological replicates). **D**) RT-PCR analysis showing the relative expression levels of miR-145-5p in CCSMCs after incubation with hASC-EVs and MT-hASC-EVs (n = 3, biological replicates). **E**) Binding sites for miR–145–5p within the 3′ untranslated region (UTR) of rat *Tgfb2* and rat *Smad3* predicted by TargeScan v8.0. **F**) Luciferase reporter activities could be inhibited by miR-145-5p mimics in 293T which are transfected with wild type *Tgfb2* and *Smad3* reporter genes, but not mutant *Tgfb2* and *Smad3* reporter genes (*n* = 3, biological replicates). **G**-**H**) Western Blot analysis showing the protein levels of TGF-β2, Smad 3 in CCSMCs after transfection with miR-145-5p mimics and inhibitor (*n* = 3, biological replicates). The six lanes are marked "a", "b", "c", "d", "e" and "f" respectively in order to simply display in (**H**). Original Western Blot bands are presented in Supplementary Fig. 7. **I**-**J**) Transfection of miR-145-5p inhibitors could impair the inhibitory effects of MT-hASC-EVs on TGF-β2/Smad3 pathway and fibrosis in CCSMCs. Western blot analysis revealed the protein levels of TGF-β2, p-Smad3, Collagen I and Collagen III in CCSMCs (*n* = 3, biological replicates). The five lanes are marked "①", "②", "③", "④" and "⑤" respectively in order to simply display in (**J**). Original Western Blot bands are presented in Supplementary Fig. 8. Data are presented as the mean ± SD. Statistical analyses are performed by Student's t test (**D**) and One-way (**H** and **J**) or Two-way (**B**, **C** and **F**) ANOVA with the Sidak's test for multiple group comparisons. *, $p < 0.05$; **, $p < 0.01$; ***, $p < 0.001$; ****, $p < 0.0001$; ns, no significance

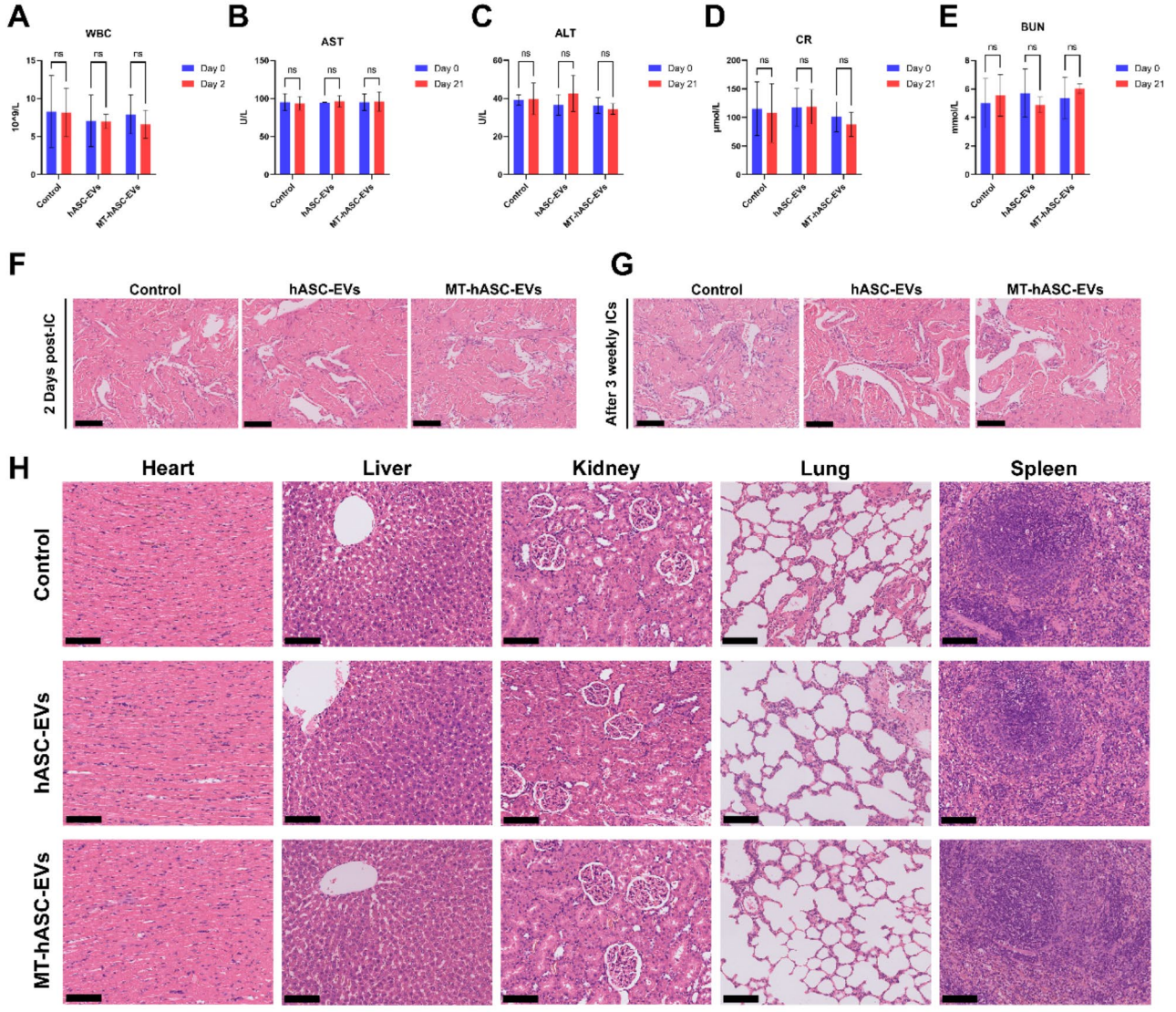

Fig. 7 Biological safety analysis of hASC-EVs and MT-hASC-EVs following a short-term (2 days) and long-term (3 weeks) observation. **A**) Analysis of white blood cells (WBC) in rat blood 2 days after intracavernous injection of hASC-EVs or MT-hASC-EVs ($n = 3$, biological replicates). **B**-**C**) Liver function analysis of rats after three weekly intracavernous injections of hASC-EVs or MT-hASC-EVs ($n = 3$, biological replicates). Aspartate aminotransferase (AST) analysis shown in (**B**). Alanine aminotransferase (ALT) analysis shown in (**C**). D-E) Kidney function analysis of rats after three weekly intracavernous injections of hASC-EVs or MT-hASC-EVs ($n = 3$, biological replicates). Creatinine (CR) analysis shown in (**D**). Blood urea nitrogen (BUN) analysis shown in (**E**). **F**) HE staining of corpus cavernosum tissue 2 days after intracavernous injection of hASC-EVs or MT-hASC-EVs. Scale bar = 100 μm. IC, intracavernous injection. **G**) HE staining of corpus cavernosum tissue after three weekly intracavernous injections of hASC-EVs or MT-hASC-EVs. Scale bar = 100 μm. **H**) HE staining of major organs of rats after three weekly intracavernous injections of hASC-EVs or MT-hASC-EVs (scale bar = 100 μm). Data are presented as the mean ± SD. Statistical analyses are performed by One-way (**G**) or Two-way (**A**, **B**, **C**, **D** and **E**) ANOVA with the Sidak's test for multiple group comparisons. *, $p < 0.05$; **, $p < 0.01$; ***, $p < 0.001$; ****, $p < 0.0001$; ns, no significance

analysis of corpus cavernosum (Fig. 7G) and key organs (Fig. 7H) did not reveal any microscopic abnormalities among the different treatment groups. In summary, MT-hASC-EVs exhibit good biocompatibility, which implies high potential for further research related to clinical translation.

Discussion

Corpus cavernosum nerve injury is one of the important causes of erectile dysfunction, commonly seen after pelvic surgery especially radical prostatectomy, with a postoperative occurrence rate of ED as high as 63-94% in two years [3]. Currently, perioperative penile rehabilitation techniques have been adopted in clinical practice, including vacuum negative pressure suction, intracavonous

injection of vasoactive agent and oral phosphodiesterase 5 inhibitors, to restore erectile function in CNI-ED patients [6]. However, about 50-75% of patients still cannot recover to their preoperative erectile function status, seriously affecting the postoperative quality of life [5]. The refractoriness of CNI-ED is closely related to its pathogenesis and development mechanism, especially severe cavernous fibrosis after CNI-ED [2]. Chronic hypoxia caused by long-term low blood flow perfusion in the penis after CNI can lead to functional impairment of corpus cavernosum smooth muscle cells through ROS accumulation [33], resulting in severely reduced responsiveness of the corpus cavernosum to nitric oxide (NO) [34]; on the other hand, hypoxia can also activate TGF-β/Smad [35] and RhoA/Rock [36] pathways leading to corporal fibrosis and impaired blood capacity and compliance. Therefore, the response effect of traditional PDE5i drugs on CNI-ED is often unsatisfactory. Thus it is urgent to study new methods for effectively targeting cavernous fibrosis in order to achieve better therapeutic effects for CNI-ED.

In recent years, many animal and clinical studies have confirmed that mesenchymal stem cells can promote recovery of erectile function in CNI-ED [8–10]. However clinically stem cell therapy for ED is still confronted with constraints such as cumbersome processes for storage, culture and proliferation; ethical issues; risk of immune rejection; tumorigenicity; pathogen contamination etc [37]. Besides, a recent study revealed that MSCs could be maintained within the cavernous tissue for only 3 days in CNI-ED rats with no obvious evidence for endothelial and smooth muscle differentiation, indicating that MSC differentiation does not play a major role in treatment efficacy [38]. The paracrine function, especially extracellular vesicles (EVs), is likely to be one of the main mechanisms for the therapeutic effects of MSCs. MSC-derived EVs exert therapeutic effects while avoiding risks associated with stem cell therapy, making them suitable for industrial preparation, thus having good prospects for clinical translation [14, 39, 40]. Therefore, in this study, we also selected EVs isolated and enriched from the conditioned medium of hASCs for intracavernous injection, in order to achieve better treatment efficiency.

Melatonin (MT) is an amine hormone mainly synthesized and secreted by the pineal gland, which has been proved to alleviate CNI-ED by promoting the repair of cavernous nerve [25, 26]. However, it should be noted that the cavernous nerve can be spontaneously repaired after CNI, while downstream cavernous fibrosis is difficult to reverse [7]. Therefore, neuroprotection and regeneration may not be the only mechanism by which melatonin exerts its therapeutic effect on CNI-ED. Many studies have demonstrated Melatonin's anti-fibrotic effects in various disease models, such as liver fibrosis [21], pulmonary fibrosis [22], renal fibrosis [23], etc. So it is reasonable to infer that the anti-fibrotic effect of Melatonin also plays a rather important role in the remission of CNI-ED, but this has not been elucidated before. In addition, melatonin can also regulate MSCs behavior and significantly enhance the therapeutic effect of EVs derived from MSCs in certain diseases [27, 28]. It has also been observed that exosomes isolated from melatonin-stimulated MSCs can to some extent alleviate renal fibrosis in chronic kidney disease [41].

In order to verify the above conjecture and clarify its intrinsic mechanism, in this study, we enriched exosomes produced by hASCs after pretreatment with melatonin. On one hand, MT-hASC-EVs contain melatonin absorbed by hASC during pretreatment which can exert a certain therapeutic effect; on the other hand and more importantly, melatonin can regulate the composition of EVs derived from hASCs, thus enhancing the therapeutic effect. Through in vivo experiments, we found that intracavernous injection of MT-hASC-EVs could significantly ameliorate the erectile function of CNI-ED rats, meanwhile reduce collagen accumulation indicated by Masson staining, and increase Desmin staining distribution in the cavernous tissue. They could also inhibit the expression of TGF-β pathway-related molecules such as TGF-β, phosphorylated-Smad3 and fibrosis marker Collagen I. Excitingly, MT-hASC-EVs have shown a more significant therapeutic effect on CNI-ED compared to the classic ED medication sildenafil. Similarly, in vitro, MT-hASC-EVs promoted the proliferation of CCSMCs, reduced hypoxia-induced apoptosis, and inhibited TGF-β2-induced fibrosis of CCSMCs by inhibiting the activation of TGF-β pathway. These experiments demonstrated the excellent anti-fibrosis ability of MT-hASC-EVs in the treatment of CNI-ED.

EVs exert regulatory effects by delivering their cargo to target cells, among which microRNAs are important components [42]. microRNAs can recognize the binding sites on the 3'-UTR of target gene mRNAs through their seed sequences (nucleotides 2–8 at the 5' end), causing the translation of mRNAs to be blocked or even degraded [43]. Therefore, to explore the underlying mechanism of the stronger therapeutic effects of MT-hASC-EVs compared to hASC-EVs, we performed high-throughput microRNA sequencing and comparison of the two types of EVs and identified 20 microRNAs with significant expression differences. Since microRNAs exert regulatory effects by downregulating the expression of target genes when they are highly expressed, the upregulated microRNAs in MT-hASC-EVs should play a more primary regulatory role, but not the down-regulated microRNAs. Thus, enrichment analysis of the target genes of upregulated miRNAs in MT-hASC-EVs revealed significant enrichment in "response to transforming growth factor

beta" and "transforming growth factor beta signaling". To identify the most crucial microRNAs, KEGG analysis by miRPath v3 suggested that miR-145-5p, miR-23a-3p, and miR-23b-3p are all related to the TGF-β pathway. Previous studies have reported the regulatory role of miR-145 in various fibrotic diseases, such as myocardial fibrosis (targeting SOX9) [44], scar hyperplasia (targeting Smad2/3) [45], liver fibrosis (targeting ADD3) [46], etc., so we chose miR-145-5p as the most likely effector molecule for further experimental design. The expression of miR-145-5p in both MT-hASCs and MT-hASC-EVs can be significantly upregulated by melatonin, confirming the conclusion of high-throughput sequencing. To clarify the downstream targets of miR-145-5p, we predicted the possible target genes of miR-145-5p using TargetScan v8.0 and sifted potential targets related to the TGF-β pathway. We identified a 7mer-A1 site for miR-145-5p in the 3'UTR of *Tgfb2* and an 8mer site in the 3'UTR of *Smad3*, which were subsequently validated using dual luciferase reporter gene assays. Finally, to verify the specificity of miR-145-5p in the anti-fibrotic effects of MT-hASC-EVs, we blocked the function of miR-145-5p by transfecting miR-145-5p inhibitor and observed a reduction in the inhibitory effects of MT-hASC-EVs on the TGF-β pathway and anti-fibrotic actions. Combining the above results, we confirmed that MT-hASC-EVs can inhibit the occurrence of fibrosis through miR-145-5p/Tgfb2/Smad3 axis.

Excitingly, MT-hASC-EVs have demonstrated good biocompatibility in biosafety testing. Multiple intracavernous injections of MT-hASC-EVs do not elicit local or systemic immune responses, nor do they adversely affect the function and structure of vital organs (heart, liver, spleen, lungs, and kidneys). As an excellent alternative to stem cell therapy, MT-hASC-EVs hold strong potential for clinical translation in the field of CNI-ED treatment.

However, our research still has some limitations worth further exploration and improvement. First, MT-hASC-EVs can promote the proliferation of CCSMCs and inhibit apoptosis in vitro, and can also increase the content of Desmin at the in vivo level, but the mechanism behind this is not yet clear. Additionally, we only focused

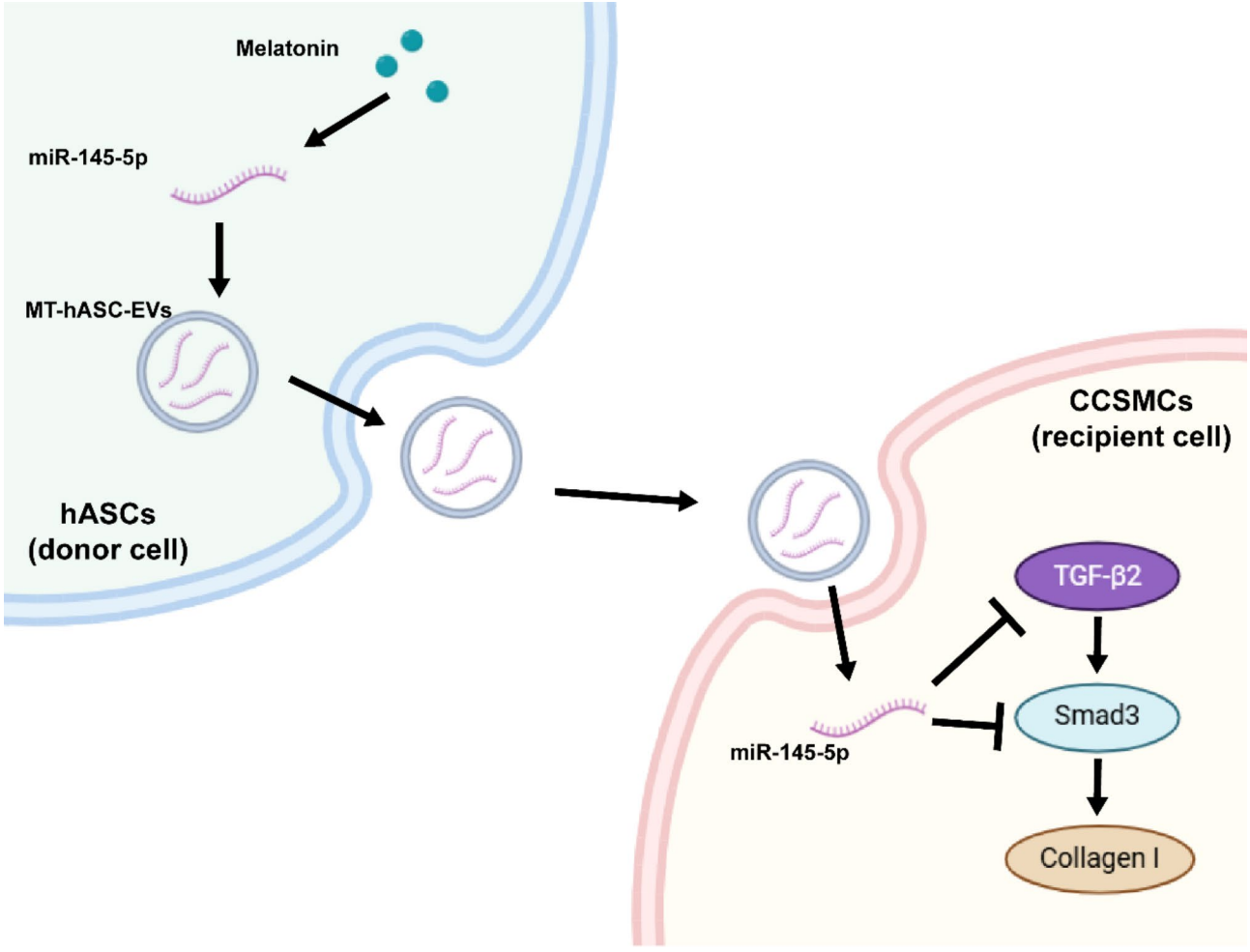

Fig. 8 MT-hASCs-EVs can significantly alleviate CNI-ED by inhibiting the occurrence of cavernous fibrosis through miR-145-5p/TGF-β/Smad axis

on the changes in the microRNA expression profile of MT-hASC-EVs, while proteins, lipids, and other molecules are also important regulatory molecules that EVs can deliver to target cells, and the potential effector molecules among them are also worth further exploration.

Conclusions

In conclusion, the present study demonstrated that intracavernous injection of MT-hASC-EVs could significantly alleviate CNI-ED. MT-hASC-EVs could effectively alleviate the apoptosis and fibrosis of CCSMCs in vitro and in vivo. Mechanistically, microRNA sequencing revealed that miR-145-5p was significantly enriched in MT-hASC-EVs and played a direct and negative regulatory role on *Tgfb2* and *Smad3* mRNAs by being transferred to CCSMCs. MT-hASCs-EVs can significantly alleviate CNI-ED by inhibiting the occurrence of fibrosis through miR-145-5p/TGF-β2/Smad3 axis (Fig. 8). All these suggest that these extracellular vesicles may be potential drugs and materials for CNI-ED treatment.

Supplementary Information

The online version contains supplementary material available at https://doi.org/10.1186/s13287-025-04173-0.

Supplementary Material 1

Supplementary Material 2

Acknowledgements
The authors declare that they have not use Artificial intelligence (AI) -generated work in this manuscript.

Author contributions
XZ and MY performed most of the experiments, analyzed the data, and drafted the manuscript. XC helped with the isolation of ASCs. MZ and YP helped with the animal experiment. ML designed this study and critically revised the manuscript. All authors have read and approved the final manuscript.

Funding
This work was supported by the National Natural Science Foundation of China (No. 82171611, No. 82371631, No. 82401887) and National Key Research and Development Program of China (2024YFA1108100).

Data availability
The original contributions presented in the study are included in the article/Supplementary Material; further inquiries can be directed to the corresponding author. The matrix of microRNA sequencing is available within the supplementary materials.

Declarations

Ethics approval and consent to participate
The study of "Application of mesenchymal stem cells in cavernous nerve injury-induced erectile dysfunction" was approved by the Ethics Committee of Renji Hospital Affiliated to Shanghai Jiao Tong University School of Medicine on Oct.26, 2022, with approval number KY2022-180-B. The patients provided written informed consent for participation in the study and the use of samples.

Consent for publication
Not applicable.

Competing interests
The authors declare that the research was conducted in the absence of any commercial or financial relationships that could be construed as a potential conflict of interest.

Received: 14 October 2024 / Accepted: 23 January 2025
Published online: 25 February 2025

References

1. Yafi FA, Jenkins L, Albersen M, Corona G, Isidori AM, Goldfarb S, et al. Erectile dysfunction. Nat Rev Dis Primers. 2016;2:16003.
2. Song G, Hu P, Song J, Liu J, Ruan Y. Molecular pathogenesis and treatment of cavernous nerve injury-induced erectile dysfunction: a narrative review. Front Physiol. 2022;13:1029650.
3. Ficarra V, Novara G, Ahlering TE, Costello A, Eastham JA, Graefen M, et al. Systematic review and meta-analysis of studies reporting potency rates after robot-assisted radical prostatectomy. Eur Urol. 2012;62:418–30.
4. Cho MC, Song WH, Paick JS. Suppression of Cavernosal Fibrosis in a rat model. Sex Med Rev. 2018;6:572–82.
5. Philippou YA, Jung JH, Steggall MJ, O'Driscoll ST, Bakker CJ, Bodie JA, et al. Penile rehabilitation for postprostatectomy erectile dysfunction. Cochrane Database Syst Rev. 2018;10:CD012414.
6. Liu C, Lopez DS, Chen M, Wang R. Penile Rehabilitation Therapy following radical prostatectomy: a Meta-analysis. J Sex Med. 2017;14:1496–503.
7. Wu YN, Chen KC, Liao CH, Chiang HS. Spontaneous regeneration of nerve Fiber and irreversibility of Corporal smooth muscle fibrosis after cavernous nerve crush Injury: evidence from Serial Transmission Electron Microscopy and Intracavernous pressure. Urology. 2018;118:98–106.
8. Yan H, Ding Y, Lu M. Current status and prospects in the treatment of Erectile Dysfunction by adipose-derived stem cells in the Diabetic Animal Model. Sex Med Rev. 2020;8:486–91.
9. Yan H, Rong L, Xiao D, Zhang M, Sheikh SP, Sui X, et al. Injectable and self-healing hydrogel as a stem cells carrier for treatment of diabetic erectile dysfunction. Mater Sci Eng C Mater Biol Appl. 2020;116:111214.
10. Haahr MK, Harken Jensen C, Toyserkani NM, Andersen DC, Damkier P, Sorensen JA, et al. A 12-Month follow-up after a single Intracavernous injection of autologous adipose-derived regenerative cells in patients with Erectile Dysfunction following radical prostatectomy: an open-label phase I clinical trial. Urology. 2018;121:203. e6-03 e13.
11. Zhang X, Yang M, Chen X, Lu M. Research progress on the therapeutic application of extracellular vesicles in erectile dysfunction. Sex Med Rev 2024.
12. Cheng L, Hill AF. Therapeutically harnessing extracellular vesicles. Nat Rev Drug Discov. 2022;21:379–99.
13. Couch Y, Buzàs EI, Di Vizio D, Gho YS, Harrison P, Hill AF et al. A brief history of nearly EV-erything – the rise and rise of extracellular vesicles. J Extracell Vesicles 2021;10.
14. Pan Z, Sun W, Chen Y, Tang H, Lin W, Chen J et al. Extracellular vesicles in tissue Engineering: Biology and Engineered Strategy. Adv Healthc Mater 2022:e2201384.
15. van Niel G, D'Angelo G, Raposo G. Shedding light on the cell biology of extracellular vesicles. Nat Rev Mol Cell Biol. 2018;19:213–28.
16. Li M, Lei H, Xu Y, Li H, Yang B, Yu C, et al. Exosomes derived from mesenchymal stem cells exert therapeutic effect in a rat model of cavernous nerves injury. Andrology. 2018;6:927–35.
17. Ouyang X, Han XY, Chen ZH, Fang JF, Huang XN, Wei HB. MSC-derived exosomes ameliorate erectile dysfunction by alleviation of corpus cavernosum smooth muscle apoptosis in a rat model of cavernous nerve injury. Stem Cell Res Ther. 2018;9:12.
18. Liang L, Shen Y, Dong ZF, Gu X. Photoacoustic image-guided corpus cavernosum intratunical injection of adipose stem cell-derived exosomes loaded polydopamine thermosensitive hydrogel for erectile dysfunction treatment. Bioact Mater. 2022;9:147–56.
19. Liu S, Li R, Dou K, Li K, Zhou Q, Fu Q. Injectable thermo-sensitive hydrogel containing ADSC-derived exosomes for the treatment of cavernous nerve injury. Carbohydr Polym. 2023;300:120226.
20. Vasey C, McBride J, Penta K. Circadian rhythm dysregulation and restoration: the role of Melatonin. Nutrients 2021;13.
21. Zhu L, Zhang Q, Hua C, Ci X. Melatonin alleviates particulate matter-induced liver fibrosis by inhibiting ROS-mediated mitophagy and inflammation via Nrf2 activation. Ecotoxicol Environ Saf. 2023;268:115717.

22. Hosseinzadeh A, Javad-Moosavi SA, Reiter RJ, Hemati K, Ghaznavi H, Mehrzadi S. Idiopathic pulmonary fibrosis (IPF) signaling pathways and protective roles of melatonin. Life Sci. 2018;201:17–29.
23. Repova K, Stanko P, Baka T, Krajcirovicova K, Aziriova S, Hrenak J, et al. Lactacystin-induced kidney fibrosis: Protection by melatonin and captopril. Front Pharmacol. 2022;13:978337.
24. Qian Y, Han Q, Zhao X, Song J, Cheng Y, Fang Z, et al. 3D melatonin nerve scaffold reduces oxidative stress and inflammation and increases autophagy in peripheral nerve regeneration. J Pineal Res. 2018;65:e12516.
25. Tavukcu HH, Sener TE, Tinay I, Akbal C, Ersahin M, Cevik O, et al. Melatonin and tadalafil treatment improves erectile dysfunction after spinal cord injury in rats. Clin Exp Pharmacol Physiol. 2014;41:309–16.
26. Zhang JL, Hui Y, Zhou F, Hou JQ. Neuroprotective effects of melatonin on erectile dysfunction in streptozotocin-induced diabetic rats. Int Urol Nephrol. 2018;50:1981–88.
27. Alzahrani FA. Melatonin improves therapeutic potential of mesenchymal stem cells-derived exosomes against renal ischemia-reperfusion injury in rats. Am J Transl Res. 2019;11:2887–907.
28. Liu W, Yu M, Xie D, Wang L, Ye C, Zhu Q, et al. Melatonin-stimulated MSC-derived exosomes improve diabetic wound healing through regulating macrophage M1 and M2 polarization by targeting the PTEN/AKT pathway. Stem Cell Res Ther. 2020;11:259.
29. Ti Y, Yang M, Chen X, Zhang M, Xia J, Lv X, et al. Comparison of the therapeutic effects of human umbilical cord blood-derived mesenchymal stem cells and adipose-derived stem cells on erectile dysfunction in a rat model of bilateral cavernous nerve injury. Front Bioeng Biotechnol. 2022;10:1019063.
30. Li Z, Yin Y, He K, Ye K, Zhou J, Qi H et al. Intracavernous pressure Recording in a cavernous nerve Injury Rat Model. J Vis Exp 2021.
31. Vlachos IS, Zagganas K, Paraskevopoulou MD, Georgakilas G, Karagkouni D, Vergoulis T, et al. DIANA-miRPath v3.0: deciphering microRNA function with experimental support. Nucleic Acids Res. 2015;43:W460–6.
32. Morikawa M, Derynck R, Miyazono K. TGF-beta and the TGF-beta family: context-dependent roles in cell and tissue physiology. Cold Spring Harb Perspect Biol 2016;8.
33. Wang HS, Ruan Y, Banie L, Cui K, Kang N, Peng D, et al. Delayed low-intensity extracorporeal shock Wave Therapy ameliorates impaired penile hemodynamics in rats subjected to Pelvic Neurovascular Injury. J Sex Med. 2019;16:17–26.
34. Karakus S, Musicki B, La Favor JD, Burnett AL. cAMP-dependent post-translational modification of neuronal nitric oxide synthase neuroprotects penile erection in rats. BJU Int. 2017;120:861–72.
35. Leungwattanakij S, Bivalacqua TJ, Usta MF, Yang DY, Hyun JS, Champion HC, et al. Cavernous neurotomy causes hypoxia and fibrosis in rat corpus cavernosum. J Androl. 2003;24:239–45.
36. Cho MC, Park K, Kim SW, Paick JS. Restoration of erectile function by suppression of corporal apoptosis, fibrosis and corporal veno-occlusive dysfunction with rho-kinase inhibitors in a rat model of cavernous nerve injury. J Urol. 2015;193:1716–23.
37. Philip S, Bredeson C, Allan DS, Altouri S, Huebsch LB, Atkins H et al. Complications and Toxicities Associated with autologous stem cell transplantation for severe autoimmune disease: single Center experience. Blood 2018;132.
38. Chen Z, Han X, Ouyang X, Fang J, Huang X, Wei H. Transplantation of induced pluripotent stem cell-derived mesenchymal stem cells improved erectile dysfunction induced by cavernous nerve injury. Theranostics. 2019;9:6354–68.
39. Witwer KW, Buzas EI, Bemis LT, Bora A, Lasser C, Lotvall J et al. Standardization of sample collection, isolation and analysis methods in extracellular vesicle research. J Extracell Vesicles 2013;2.
40. Keshtkar S, Azarpira N, Ghahremani MH. Mesenchymal stem cell-derived extracellular vesicles: novel frontiers in regenerative medicine. Stem Cell Res Ther. 2018;9:63.
41. Yea JH, Yoon YM, Lee JH, Yun CW, Lee SH. Exosomes isolated from melatonin-stimulated mesenchymal stem cells improve kidney function by regulating inflammation and fibrosis in a chronic kidney disease mouse model. J Tissue Eng 2021;12.
42. Herrmann IK, Wood MJA, Fuhrmann G. Extracellular vesicles as a next-generation drug delivery platform. Nat Nanotechnol. 2021;16:748–59.
43. Miao Y, Fu C, Yu Z, Yu L, Tang Y, Wei M. Current status and trends in small nucleic acid drug development: leading the future. Acta Pharm Sin B. 2024;14:3802–17.
44. Cui S, Liu Z, Tao B, Fan S, Pu Y, Meng X, et al. miR-145 attenuates cardiac fibrosis through the AKT/GSK-3beta/beta-catenin signaling pathway by directly targeting SOX9 in fibroblasts. J Cell Biochem. 2021;122:209–21.
45. Shen W, Wang Y, Wang D, Zhou H, Zhang H, Li L. Mir-145-5p attenuates hypertrophic scar via reducing Smad2/Smad3 expression. Biochem Biophys Res Commun. 2020;521:1042–48.
46. Ye Y, Li Z, Feng Q, Chen Z, Wu Z, Wang J, et al. Downregulation of microRNA-145 may contribute to liver fibrosis in biliary atresia by targeting ADD3. PLoS ONE. 2017;12:e0180896.

Publisher's note